Magnetic Phase Transition, Elastic and Thermodynamic Properties of L1$_2$-(Ni,Cu)$_3$(Al,Fe,Cr) in 3d High-Entropy Alloys

Li Ma [1], **Zhi-Peng Wang** [2], **Guo-Hua Huang** [1], **Jin-Li Huang** [1], **Ping-Ying Tang** [1,*] and **Tou-Wen Fan** [2,*]

[1] Key Laboratory of New Electric Functional Materials of Guangxi Colleges and Universities, Nanning Normal University, Nanning 530023, China; 20180744@nnnu.edu.cn (L.M.); hgh9@263.net (G.-H.H.); hj20130503@163.com (J.-L.H.)

[2] School of Material Science and Energy Engineering, Foshan University, Foshan 528001, China; wangzp1205@hnu.edu.cn

[*] Correspondence: tangpy@nnnu.edu.cn (P.-Y.T.); fantouwen_1980@163.com (T.-W.F.)

check for updates

Abstract: The phase stability and elastic properties of paramagnetic (PM), ferromagnetic (FM) and antiferromagnetic (AFM) phases in L1$_2$-(Ni,Cu)$_3$(Al,Fe,Cr) alloy are first investigated using the exact muffin-tin orbitals (EMTO) method in combination with the coherent potential approximation (CPA). The result shows the AFM structure phase of the three is the most stable in the ground state. Calculated elastic constants show that all the phases are mechanically stable, and have uncovered that L1$_2$-(Ni,Cu)$_3$(Al,Fe,Cr) can achieve good strength and ductility simultaneously. Then, crucial thermal properties are described satisfactorily using the Debye–Grüneisen model, showing heat capacity, Gibbs free energy G, the competitive contribution of entropy $-TS$ and enthalpy H exhibiting significant temperature dependences. Moreover, the magnetic phase transition thermodynamics was studied, which suggests that $-TS$ has a primary contribution to Gibbs free energy and may play a key role in the phase transition. The present results can benefit the understanding of the mechanical, thermodynamic and magnetic properties of the L1$_2$ structure phase in 3d high-entropy alloys.

Keywords: L1$_2$ structure; high-entropy alloys; elastic properties; thermodynamic properties; magnetic phase transition

1. Introduction

High-entropy alloys (HEAs), near-equiatomic solid solutions of five or more elements, represent a new strategy for the design of materials with properties superior to those of conventional alloys. [1,2]. With multiple principal components, they inherently possess unique microstructures and many impressive properties, such as high strength and hardness, excellent magnetic property, thermal stability, wear-resistance and corrosion resistance [3–5]. Although HEAs often form single-phase alloys because of a high configuration entropy of mixing, such as a simple face-centered cubic (FCC) or body-centered cubic (BCC) structure [6,7], intermetallic compound precipitates with B$_2$, L1$_2$ or L2$_1$ structures are observed in HEAs through X-ray diffraction (XRD) and transmission electron microscopes (TEM) measurements [8–10]. These phases are beneficial to the mechanical behavior of HEAs. For instance, the ordered L1$_2$-(Ni,Cu)$_3$(Al,Fe,Cr) phase (γ′ phase), which has been obtained by annealing of Al$_{0.3}$CuCrFeNi$_2$ at 550–700 °C, could improve the mechanical strength, grain refinement, microstructures and coarsening behavior of HEAs [8]. These favorable properties seem to originate from the γ′ precipitates uniformly distributed within a disordered FCC solid solution matrix of HEAs, mimicking typical γ + γ′ microstructures observed in the case of many Ni-super alloy and forms the basis

of the excellent high temperature mechanical properties of these alloys. Therefore, the investigations of L1$_2$ precipitates are crucial for designing potential high temperature 3d-HEAs. However, up to now, little is known about phase stability, elastic and thermodynamic properties for L1$_2$-(Ni,Cu)$_3$(Al,Fe,Cr) precipitate. Moreover, the L1$_2$-(Ni,Cu)$_3$(Al,Fe,Cr) phase includes magnetic transition elements Ni, Cu, Cr and Fe, the investigation of magnetism in the (Ni,Cu)$_3$(Al,Fe,Cr) phase is also significant.

In the present work, the exact muffin-tin orbitals (EMTO) method [11,12] in combination with coherent potentials approximation (CPA) [13] are employed to investigate the phase stability and elastic properties of the paramagnetic (PM), ferromagnetic (FM) and antiferromagnetic (AFM) phases in L1$_2$-(Ni,Cu)$_3$(Al,Fe,Cr). The quasi-harmonic Debye–Grüneisen approach [14] has turned out to be valid in describing the temperature-dependent thermodynamic properties. Specially, magnetic phase transition is predicted by Gibbs free energy G and the competitive contribution of entropy $-TS$ and enthalpy H, simultaneously.

2. Computational Details

The EMTO–CPA method [11–13] within the framework of density functional theory (DFT), is used for total energies calculations, as this method has proved to be very useful to study the equilibrium properties of HEAs [15–17]. Within the EMTO theory, the single-electron equations were solved for the optimized overlapping muffin-tin potential and the full charge density technique [18] was used to compute the total energy. Generalized gradient approximation (GGA) of Perdew–Burke–Ernzerhof (PBE) was used for the exchange correlation functional [19], and the Brillouin zone integrations were performed on $17 \times 17 \times 17$ k-points mesh. The electrostatic correction to the single-site CPA was described using the screened impurity model with a screening parameter 0.9 [20]. In our calculations, the atomic proportions of Ni, Cu, Al, Fe and Cr in (Ni,Cu)$_3$(Al,Fe,Cr) were designed as 37.50%, 37.50%, 8.33%, 8.33% and 8.34%, respectively. Here we employed the disordered local magnetic moment (DLM) model [21–23] to describe the magnetic states of HEAs. According to the model, an alloy component M of concentration m is presented by its spin-up (↑) and spin-down (↓) counterparts assumed to be distributed randomly on the underlying sublattice; i.e., each magnetic alloy component could be treated as $M^{\uparrow}_{m/2}M^{\uparrow}_{m/2}$ (FM) and $M^{\downarrow}_{m/2}M^{\downarrow}_{m/2}$ (AFM).

3. Results and Discussion

3.1. Phase Stability

In order to check for the structural stability in paramagnetic (PM), ferromagnetic (FM) and antiferromagnetic (AFM) phases for L1$_2$-(Ni,Cu)$_3$(Al,Fe,Cr), the total energies are calculated as a function of unit cell volume and fitted to Birch Murnaghan equation of state (BM3-EOS) [24]. The obtained energy versus volume curves are shown in Figure 1. It can be clearly seen that the L1$_2$-(Ni,Cu)$_3$(Al,Fe,Cr) is stable in the AFM phase in the ground state because it shows the lowest total energy of the AFM configuration corresponding to the equilibrium lattice constant. Interestingly, the curves have three intersection in the figure, implying that magnetic phase transition among PM, FM and AFM phases for L1$_2$-(Ni,Cu)$_3$(Al,Fe,Cr) would probably happen under high temperature and high pressure, which are discussed in Section 3.3.
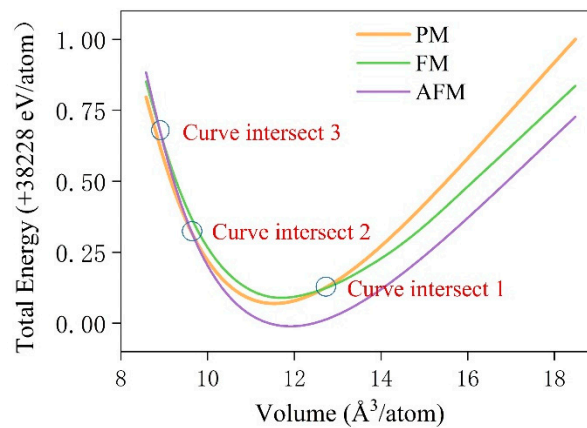
Figure 1. The energy versus volume curves of paramagnetic (PM), ferromagnetic (FM) and antiferromagnetic (AFM) phases for L1$_2$-(Ni,Cu)$_3$(Al,Fe,Cr).

To further determine the phase stability, the mixing energies (E_{mix}) against the different magnetic configurations HEAs are also calculated from the following equation:

$$E_{mix} = (E_{tot} - \sum_i N_i E^i_{solid}) / \sum_i N_i \tag{1}$$

where E_{tot} is the total energy per atom of the HEAs and E^i_{solid} is the energy per atom of ith composition in fcc structure, N_i refers to the atom number of ith composition in the HEAs. The calculation mixing energies E_{mix} are, respectively, -8.95, -8.97 and -8.98 ev for PM, FM and AFM structures (Ni,Cu)$_3$(Al,Fe,Cr). The negative mixing energies E_{mix} prove that of all the phases of HEAs are stable at zero temperature and zero pressure. Moreover, the values of E_{mix} demonstrate the order of PM > FM > AFM, suggesting the AFM structure phase is the energetically favorable phase at low temperature, while PM structure phase is the most instable. Additionally, the magnetic phase transition may easily occur due to the small difference in E_{mix} for the different magnetic structures (Ni,Cu)$_3$(Al,Fe,Cr).

3.2. Elastic Properties

The elastic constants and moduli provide important parameters of mechanical properties, such as stability, stiffness of materials and nature of interatomic forces. Hence, the study of the elastic properties of different magnetic structures (Ni,Cu)$_3$(Al,Fe,Cr) are necessary. The elastic constants (C_{11}, C_{12} and C_{44}) are calculated through the small strains to the equilibrium unit cell and determined by the corresponding variations in the total energy [25], and the elastic moduli (B, G, and E) are derived by means of the Voigt–Reuss–Hill approximation [26]. As a result, the obtained elastic constants and elastic moduli are summarized in Table 1. It is noted that all the elastic constants meet the corresponding mechanical stability criteria [27,28]: $C_{11} - C_{12} > 0$, $C_{11} > 0$, $C_{44} > 0$, $C_{11} + 2C_{12} > 0$, and $C' = (C_{11} - C_{12})/2 > 0$. This implies all the structures (Ni,Cu)$_3$(Al,Fe,Cr) are mechanically stable, which agree with the conclusion obtained from the mixing energies above.

Generally, bulk modulus B indicates the compressibility of the solid under hydrostatic pressure, which can be also used to describe the strength of materials. Calculated bulk modulus B shows that all phases of L1$_2$-(Ni,Cu)$_3$(Al,Fe,Cr) are stronger due to large bulk modulus. Close comparison shows that the B of the PM structure (Ni,Cu)$_3$(Al,Fe,Cr) is the highest, indicating strongest compression resistance compared to the FM and AFM structure HEAs. Moreover, shear modulus G is more relevant to hardness compared to B, which is defined as the force that resists shape change under shear stress [29,30]. The order of G is as follows: PM < FM < AFM, indicating that the hardness of the PM and AFM structure phases are the lowest and highest in these HEAs, respectively. In addition, the Young's modulus E is regarded as a standard of solid stiffness, and the higher Young's modulus

corresponds to the stiffer solid. As seen in Table 1, the AFM structure HEA has the largest *E* among these HEAs, which means that the AFM structure phase is the stiffest compound.

It is well known that the ductility and brittleness of alloys are related to the values of Pugh's modulus ratio *G/B* Cauchy pressure $C_{12} - C_{44}$ and Poisson ratio *v*. If a material exhibits ductility, the alloy should meet the following requirements: $G/B < 0.57$, $C_{12} - C_{44} > 0$ and $v > 0.26$ [27,31,32]. Generally, the larger the $C_{12} - C_{44}$ and *v* and the smaller the *G/B*, the more ductile the material is [31]. The calculated *G/B*, $C_{12} - C_{44}$ and *v* of different magnetic structures $(Ni,Cu)_3(Al,Fe,Cr)$ are also shown in Table 1. It is obvious that, for all magnetic structures $(Ni,Cu)_3(Al,Fe,Cr)$, their *G/B*, $C_{12} - C_{44}$ and *v* values obey the ductile conditions, indicating that these HEAs are ductile. Moreover, PM structures $(Ni,Cu)_3(Al,Fe,Cr)$ are the most ductile due to the largest $C_{12} - C_{44}$ and *v* and the smallest *G/B*.

Table 1. Calculated ground state and elastic properties of PM, FM and AFM phases of $(Ni,Cu)_3(Al,Fe,Cr)$.

	C_{11}	C_{12}	C_{44}	*B*	*G*	*E*	*v*	*G/B*	$C_{12}-C_{44}$
PM	213.7	166.4	118.3	182.2	80.5	210.4	0.308	0.44	48.1
FM	187.8	141.5	118.9	156.9	85.6	206.4	0.281	0.55	22.6
AFM	193.9	148.1	128.0	163.4	86.0	219.4	0.276	0.52	20.1

3.3. Thermodynamic Properties and Magnetic Phase Transition

The thermal property provides valuable information on the specific performance of solids under the application of temperature, and it plays a very important role in helping understanding on phase transition. In this paper, the quasi-harmonic Debye model [14] in the temperature range of 0 to 1200 K and pressure range of 0 to 60 GP is studied to derive thermodynamic properties of three magnetic phases in $L1_2$-$(Ni,Cu)_3(Al,Fe,Cr)$, as this method has been successfully applied to various thermodynamic calculations [33]. The knowledge of the heat capacity is one of the most important thermodynamic properties which not only provides essential insight into its vibrational properties but also is mandatory for many applications [33]. Figure 2 shows the heat capacities at a constant volume (C_V) of PM, FM and AFM phases for $L1_2$-$(Ni,Cu)_3(Al,Fe,Cr)$ as functions of the temperature under 0 GP. As it can be seen, all magnetic configuration HEAs show the same changing trend with increasing temperature: C_V is proportional to T^3 at low temperature and converges to the Dulong–Petit limit at high temperature, which obeys the change law. It is should be noted that the concentration of magnetic behavior has little influence on the heat capacity behavior, due to the values of C_V of all phases for $(Ni,Cu)_3(Al,Fe,Cr)$ being extremely similar. In other words, the C_V is not sensitive to the presence of magnetism as the temperature increases.
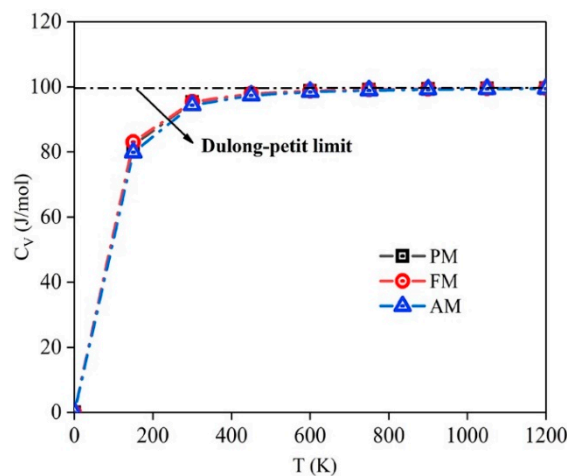
Figure 2. The isochoric heat capacity (C_v) of PM, FM and AFM phases for $L1_2$-$(Ni,Cu)_3(Al,Fe,Cr)$.

　　　In order to investigate magnetic phase transition of the $L1_2$-(Ni,Cu)$_3$(Al,Fe,Cr), the Gibbs free energy G as a function of temperature at constant pressures was calculated by the equation $G = H - TS$, and the two components of enthalpy H and entropy contribution $-TS$ were also studied, which are shown in Figures 3 and 4. It is clear that from Figure 3, for all phases, the variation tendency of the H and $-TS$ at 20, 30 and 40 GPa are, to some extent, similar. The H increases as the temperature increases, while the $-TS$ monotonously decreases. As pressures rise, the values of H and $-TS$ of all phases for $L1_2$-(Ni,Cu)$_3$(Al,Fe,Cr) are very close, this means the concentration of magnetic behavior has little influence on the H and $-TS$ at high pressure; this is because magnetism in *3d* metals is typically suppressed by the application of pressure [34,35]. Figure 4 shows that as the pressure increases, the G values increase, demonstrating that high pressure significantly affects the system energy and reduces the stability of HEAs. Moreover, upon comparison of the values of G, H and $-TS$, the variation tendency of G is the same as the $-TS$, but contrary to the H, suggesting that $-TS$ has a primary contribution to Gibbs free energy, that is to say that the entropy may play a key role in the phase transition in the annealing process.

　　　Generally, the smaller the G, the more stable the material is. It should be noted that in Figure 4 there are two energetically favorable phases from 0 to 1200 K under 20 and 40 GPa, showing that the magnetic phase transformation will occur from the AFM to FM phase in the temperature range of 900 to 1050 K at 20 GPa, and from the AFM to PM phase in the temperature range of 150 to 300 K at 40 GPa, respectively. In particular, the tow phase transformation will occur under 30 GPa; the phase change temperatures are 450~600 and 1050~1050 K, respectively.
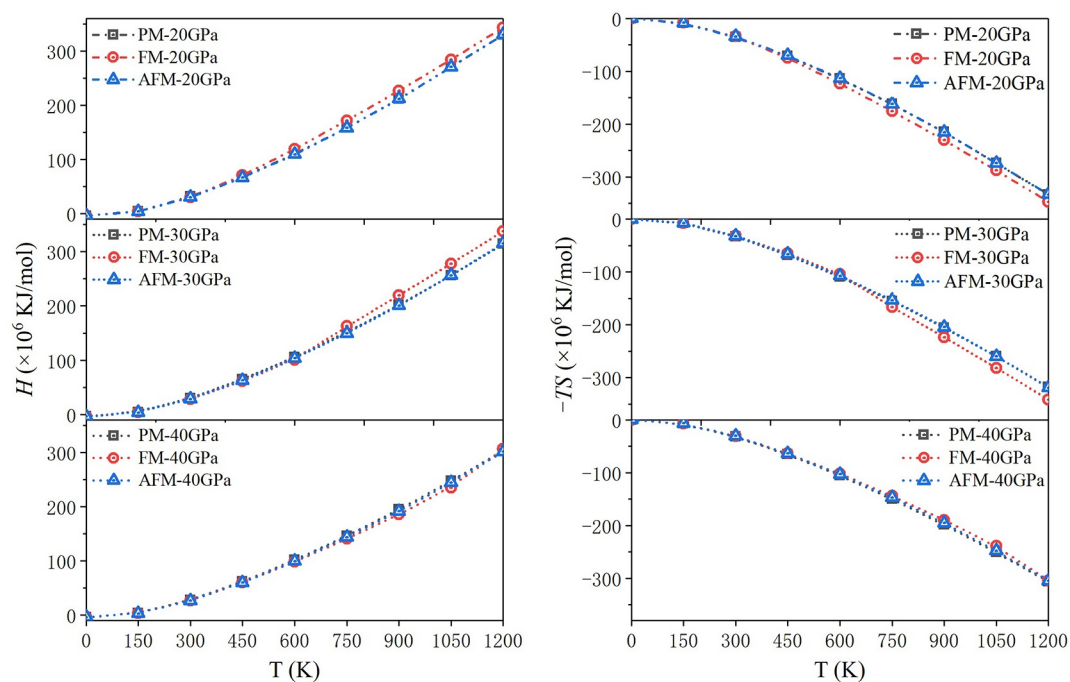
Figure 3. The enthalpy H(T), entropy contribution to free energy $-TS$(T) of the PM, FM and AFM phases for $L1_2$-(Ni,Cu)$_3$(Al,Fe,Cr) at 20, 30 and 40 GPa.
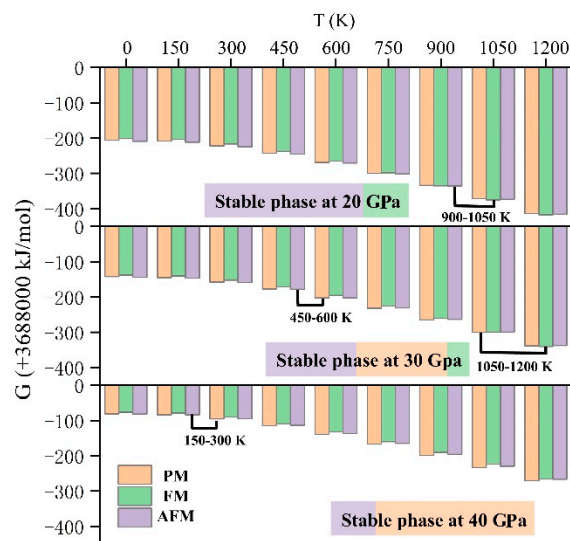
Figure 4. The Gibbs free energy *G* (T) of the PM, FM and AFM phases for (Ni,Cu)$_3$(Al,Fe,Cr) at 20, 30 and 40 GPa.

4. Conclusions

The phase stability, elastic and thermodynamic properties and magnetic phase transition of L1$_2$-(Ni,Cu)$_3$(Al,Fe,Cr) in 3*d* high-entropy alloys were investigated employing by EMTO–CPA in combination with the quasi-harmonic Debye–Grüneisen model. The calculated total energies and mixing energies show that all the magnetic structures of L1$_2$-(Ni,Cu)$_3$(Al,Fe,Cr) are stable, and the AFM structure phase is the energetically favorable phase in the ground state. The calculated elastic constants satisfy the stability criteria, implying that all the structures (Ni,Cu)$_3$(Al,Fe,Cr) are mechanically stable. In particular, L1$_2$-(Ni,Cu)$_3$(Al,Fe,Cr) shows both good strength and extensibility due to the large bulk modulus *B* and Poisson ratio *ν*. The thermodynamic property investigation shows that the temperature has a significant effect on heat capacity, Gibbs free energy *G* and the competitive contribution of entropy −*TS* and enthalpy *H*. As pressures rise, the concentration of magnetic behavior has little influence on the *H* and −*TS* at high pressure due to pressure-induced suppression magnetism in 3*d* HAEs. Evidently, our present work may be valuable for understanding the mechanical, thermodynamic and magnetic properties of the L1$_2$ structure phase in 3*d* high-entropy alloys.

Author Contributions: Conceptualization, L.M. and T.-W.F.; formal analysis, L.M.; data curation, Z.-P.W.; validation, Z.-P.W. and G.-H.H.; resources, Z.-P.W.; investigation, J.-L.H. and P.-Y.T. They contributed to discussions and reviewed the manuscript. All authors have read and agreed to the published version of the manuscript.

Conflicts of Interest: The authors declare no conflict of interest.

References

1. Ye, Y.F.; Wang, Q.; Lu, J.; Liu, C.T.; Yang, Y. High-entropy alloy: Challenges and prospects. *Mater. Today* **2016**, *19*, 349–362. [CrossRef]
2. Laplanche, G.; Berglund, S.; Reinhart, C.; Kostka, A.; George, E.P. Phase stability and kinetics of σ-phase precipitation in CrMnFeCoNi high-entropy alloys. *Acta Mater.* **2018**, *161*, 338–351. [CrossRef]
3. Fu, Z.; Chen, W.; Wen, H.; Zhang, D.; Chen, Z.; Zheng, B.; Zhou, Y.; Lavernia, E. Microstructure and strengthening mechanisms in an FCC structured single-phase nanocrystalline Co25Ni25Fe25Al7.5Cu17.5 high-entropy alloy. *Acta Mater.* **2016**, *107*, 59–71. [CrossRef]

4. Zhou, Y.J.; Zhang, Y.; Wang, Y.L.; Chen, G.L. Solid solution alloys of AlCoCrFeNiTix with excellent room-temperature mechanical properties. *Appl. Phys. Lett.* **2007**, *90*, 253–256. [CrossRef]

5. Shon, Y.; Joshi, S.S.; Katakam, S.; Rajamure, R.S.; Dahotre, N.B. Laser additive synthesis of high entropy alloy coating on aluminum: Corrosion behavior. *Mater. Lett.* **2015**, *142*, 122–125. [CrossRef]

6. Senkov, O.N.; Scott, J.M.; Senkova, S.V.; Miracle, D.B.; Woodward, C.F. Microstructure and room temperature properties of a high-entropy TaNbHfZrTi alloy. *J. Alloys Compd.* **2011**, *509*, 6043–6048. [CrossRef]

7. Yong, D.; Lu, Y.; Li, J.; Wang, T.; Li, T. Effects of electro-negativity on the stability of topologically close-packed phase in high entropy alloys. *Intermetallics* **2014**, *52*, 105–109.

8. Gwalani, B.; Soni, V.; Choudhuri, D.; Lee, M.; Hwang, J.Y.; Nam, S.J.; Ryu, H.; Hong, S.H.; Banerjee, R. Stability of ordered $L1_2$ and B_2 precipitates in face centered cubic based high entropy alloys—$Al_{0.3}CoFeCrNi$ and $Al_{0.3}CuFeCrNi_2$. *Scripta Mater.* **2016**, *123*, 130–134. [CrossRef]

9. Liu, S.; Cao, P.; Lin, D.; Tian, F. Stability of L21 (NiM)2TiAl (M = Co, Fe) in high-entropy alloys. *J. Alloys Compd.* **2018**, *764*, 650–655. [CrossRef]

10. Choudhuri, D.; Alam, T.; Borkar, T.; Gwalani, B.; Mantri, A.S.; Srinivasan, S.G.; Gibson, M.A.; Banerjee, R. Formation of a Huesler-like L2 1 phase in a CoCrCuFeNiAlTi high-entropy alloy. *Scripta Mater.* **2015**, *100*, 36–39. [CrossRef]

11. Vitos, L. Total-energy method based on the exact muffin-tin orbitals theory. *Phys. Rev. B Condens. Matter* **2001**, *64*, 167–173. [CrossRef]

12. Vitos, L.; Skriver, H.L.; Johansson, B.; Kollár, J. Application of the exact muffin-tin orbitals theory: The spherical cell approximation. *Comput. Mater Sci.* **2012**, *18*, 24–38. [CrossRef]

13. Vitos, L.; Abrikosov, I.A.; Johansson, B. Anisotropic lattice distortions in random alloys from first-principles theory. *Phys. Rev. Lett.* **2001**, *87*, 156401. [CrossRef]

14. Otero-De-La-Roza, A.; Abbasi-Pérez, D.; Luaña, V. GIBBS2: A new version of the quasiharmonic model code. II. Models for solid-state thermodynamics, features and implementation. *Comput. Phys. Commun.* **2011**, *182*, 2232–2248. [CrossRef]

15. Tian, F.; Delczeg, L.; Chen, N.; Varga, L.K.; Shen, J.; Vitos, J. Structural stability of NiCoFeCrAlx high-entropy alloy from ab initio theory. *Phys. Rev. B* **2013**, *88*, 1336–1340. [CrossRef]

16. Tian, F.; Varga, L.K.; Chen, N.; Shen, J.; Vitos, L. Ab initio design of elastically isotropic TiZrNbMoVx high-entropy alloys. *J. Alloys Compd.* **2014**, *599*, 19–25. [CrossRef]

17. Cao, P.; Ni, X.; Tian, F.; Varga, L.K.; Vitos, L. Ab initio study of Al x MoNbTiV high-entropy alloys. *J. Phys. Condens. Matter* **2015**, *27*, 075401. [CrossRef]

18. Vitos, L. *Computational Quantum Mechanics for Materials Engineers*; Springer: Berlin/Heidelberg, Germany, 2007.

19. Perdew, P.J.; Burke, K.; Ernzerhof, M. Generalized Gradient Approximation Made Simple. *Phys. Rev. Lett.* **1996**, *77*, 3865–3868. [CrossRef]

20. Korzhavyi, P.A.; Ruban, A.V.; Abrikosov, I.A.; Skriver, H.L. Madelung energy for random metallic alloys in the coherent potential approximation. *Phys. Rev. B* **1995**, *51*, 5773–5776. [CrossRef]

21. Staunton, J.; Gyorffy, B.L.; Pindor, A.J.; Stocks, G.M.; Winter, H. The "disordered local moment" picture of itinerant magnetism at finite temperatures. *J. Magn. Magn. Mater.* **1984**, *45*, 15–22. [CrossRef]

22. Li, X.; Schönecker, S.; Zhao, J.; Johansson, B.; Vitos, L. Elastic properties of Fe–Mn random alloys studied by ab initio calculations. *J. Alloys Compd.* **2007**, *91*, 3124–3161.

23. Tian, F.; Varga, L.K.; Chen, N.; Delczeg, L.; Vitos, L. Ab initio investigation of high-entropy alloys of 3d elements. *Phys. Rev. B* **2013**, *87*, 178–187. [CrossRef]

24. Birch, F. Finite Strain Isotherm and Velocities for Single Crystal and Polycrystalline NaCl at High Pressure and 300 K. *J. Geophys. Res.* **1978**, *83*, 1257–1268. [CrossRef]

25. Mattesini, M.; Ahuja, R.; Johansson, B. Cubic Hf3N4 and Zr3N4: A class of hard materials. *Phys. Rev. B* **2003**, *68*, 184108. [CrossRef]

26. Hill, R. The Elastic Behaviour of a Crystalline Aggregate. *Proc. Phys. Soc.* **1952**, *65*, 349–354. [CrossRef]

27. Huang, B.; Duan, Y.H.; Sun, Y.; Peng, M.J.; Chen, S. Electronic structures, mechanical and thermodynamic properties of cubic alkaline-earth hexaborides from first principles calculations. *J. Alloys Compd.* **2015**, *635*, 213–224. [CrossRef]

28. Chouhan, S.S.; Pagare, G.; Rajagopalan, M.; Sanyal, S.P. First principles study of structural, electronic, elastic and thermal properties of YX (X = Cd, In, Au, Hg and Tl) intermetallics. *Solid State Sci.* **2012**, *14*, 1004–1011. [CrossRef]

29. Ivanovskii, A.L. Mechanical and electronic properties of diborides of transition 3d–5d metals from first principles: Toward search of novel ultra-incompressible and superhard materials. *Prog. Mater. Sci.* **2012**, *57*, 184–228. [CrossRef]

30. Teter, D.M. Computational Alchemy: The Search for New Superhard Materials. *MRS Bull.* **1998**, *23*, 22–27. [CrossRef]

31. Wei, Z.; Bao, D.L.; Ping, L.; Duan, Y. Elastic Anisotropies and Thermal Properties of Cubic TMIr (TM = Sc, Y, Lu, Ti, Zr and Hf): A DFT Calculation. *Mater. Res. Express* **2019**, *6*, 086574.

32. Pugh, S.F. XCII. Relations between the elastic moduli and the plastic properties of polycrystalline pure metals. *Philos. Mag.* **2009**, *45*, 823–843. [CrossRef]

33. Lu, Z.W.; Zhou, D.W.; Bai, J.P.; Lu, C.; Zhong, Z.G.; Li, G.Q. Theoretical investigation on structural and thermodynamic properties of the intermetallic compound in Mg–Zn–Ag alloy under high pressure and high temperature. *J. Alloys Compd.* **2013**, *550*, 406–411. [CrossRef]

34. Iota, V.; Klepeis, J.H.P.; Yoo, C.S.; Lang, J.; Srajer, G. Electronic structure and magnetism in compressed 3d transition metals. *Appl. Phys. Lett.* **2007**, *90*, 1560. [CrossRef]

35. Tracy, C.L.; Park, S.; Rittman, D.R.; Zinkle, S.J.; Bei, H.; Lang, M.; Ewing, R.C.; Mao, W.L. High pressure synthesis of a hexagonal close-packed phase of the high-entropy alloy CrMnFeCoNi. *Nat. Commun.* **2017**, *8*, 15634. [CrossRef]